Structural and optical properties of rare earth (Sm^{3+})-doped hematite nanostructures

Ntokozo G Cebekhulu[1], Ceboliyazakha L Ndlangamadla[1], Prince S Mkwae[1], Donald D Hile [1],[3] Sipho E Mavudla[2], and Siphamandla Masekane [2]

[1]Department of Physics, University of Zululand, KwaDlangezwa Campus, KwaZulu-Natal, South Africa.
[2] Department of Chemistry, University of Zululand, KwaDlangezwa Campus, KwaZulu-Natal, South Africa.
[3]Department of Physics, Joseph Sarwuan Tarka University, Makurdi, Nigeria.

E-mail: Ntokozongc200@gmail.com

Abstract. Samarium (Sm^{3+})(0-6%) doped hematite (α-Fe_2O_3) nanostructure were synthesized using the hydrothermal method and characterized to evaluate structural and optical modifications. X-ray diffraction confirmed the rhombohedral of α-Fe_2O_3 structure in the 3RC spacing group with reduced crystallite size upon the (Sm^{3+}) doping. Transmission electron microscopy revealed morphology changes from spherical particles to nanords with increasing dopant concentration. Fourier transform infrared spectroscopy verified Fe-O bonding and indicated a shift in the transmittance due to Sm^{3+} incorporation. Ultraviolet-visible spectroscopy analysis shows a progressive band gap narrowing from 2.23 eV to 1.81 eV as Sm^{3+} content increased, enhancing light absorption. The observed structural and optical transformations suggest the potential of Sm^{3+}-doped α-Fe_2O_3 for improved performance in optoelectronic and sensing applications.

1. Introduction

Hematite (α-Fe_2O_3) has been viewed as one of the promising materials in different applications such as gas sensing, water purification, and solar cells[1]. This material shows the crystalline structure, which is rhombohedral in the 3Rc space group, with the band gap energy typically ranging from 1.9 - 2.2 eV. α-Fe_2O_3 is a non-toxic material, low cost, and it is more stable at temperatures below 657 [2][3]. However, based on a previous reported study on hematite, it is clear that there is a noticeable gap in the performance of this material. High operating temperature conditions, low response, and long stability tend to cause problems for hematite material. This study aims to fulfil the gap on the α-Fe_2O_3 material. Based on the existing reported works, there are many methods of improving the properties of the materials, which include decorating the material with other elements such as palladium, forming the heterojunction structure (n-n),(p-p), and (n-p). Another effective method is through doping with other elements. This work reports an investigation of the effect of doping with the rare earth element on the α-Fe_2O_3 material [4][5]. This is mainly because most rare earth elements can enhance the properties of the material when used as dopant materials.

2. Experimental method

Hydrothermal synthesis was used as the main method for preparing the undoped and Sm^{3+} doped α-Fe_2O_3 materials. The starting materials are as follows: Iron chloride purity 99%, distilled water, ammonia solution, samarium, and ethanol. The calculated mass of the iron source was mixed with distilled water using a magnetic stirrer to form the solution, and the pH was kept at a value of 8 for all prepared samples. The ammonia solution was added dropwise to the prepared solution to form the precipitate. As-prepared solution was transferred into the autoclave system, and it was heated at the operating temperature of 160 °C for 4hr. After the reaction was completed the autoclave was allowed to cool naturally at room temperature. The as-prepared solution was then washed in a centrifuge using distilled water and ethanol. The final product was dried in an oven for 4hr and it was also calcined in open air with a temperature of 500 °C on the Furnace system to obtain the α-Fe_2O_3 materials. For the Sm^{3+}-doped samples, the same procedure was repeated but with the addition of different percentages (2, 4, and 6%) of Sm^{3+} ions.

3. Characterization Techniques

The structural properties of α-Fe_2O_3, and Sm^{3+}-α-Fe_2O_3 doped were characterized using X-ray diffraction (XRD), which used $Cu/K\alpha$ radiation as the source and the wavelength of $\lambda = 1.5418$ Å[6]. The morphology was analyzed using transmission electron microscopy (TEM). The chemical bonding of the undoped and doped material was investigated using the Fourier transform infrared (FT-IR) spectroscopy instrument, while the pore size distribution was further investigated using the BET instrument. The optical properties were carried out using Ultraviolet-visible (UV-Vis) spectroscopy with a wavelength range from 200 - 800 nm.

4. Result and Discussion

4.1. XRD analysis

The (XRD) pattern displayed in Figure 1 shows the diffraction peaks corresponding to nanoparticles of α-Fe_2O_3 NPs with the peaks allocated to the (012), (104),(110),(113),(024),(116),(214) and (300) planes, confirming the Rhombohedral structure in R3c space group.Figure 2 represents the zoomed pattern of the XRD for the most intense peaks to further study the influence of doping with Sm^{3+} on α-Fe_2O_3 Np. The crystallite size (D) of the undoped and Sm^{3+}-doped materials was determined using Scherrer's equation respectively [7][8].

$$D = \frac{K\lambda}{\beta \cos\theta} \tag{1}$$

Where D is crystallite size in nanometers (nm),k is the shape constant ranges from 0.9-1, λ is the wavelength of the XRD, β is the full width at half maximum (FWHM), and θ represents the braggs angles in (radians). Other important parameters, such as microstrain and dislocation density, were calculated, respectively, to investigate the effect of Sm^{3+} doping using the following equations:

$$\varepsilon = \frac{\beta_{\text{strain}}}{4 \tan\theta} \tag{2}$$

$$\delta = \frac{1}{D^2} \tag{3}$$

The raw data calculated from the Scherrer equation, microstrain, and dislocation density are shown in Table 1 for further analysis.

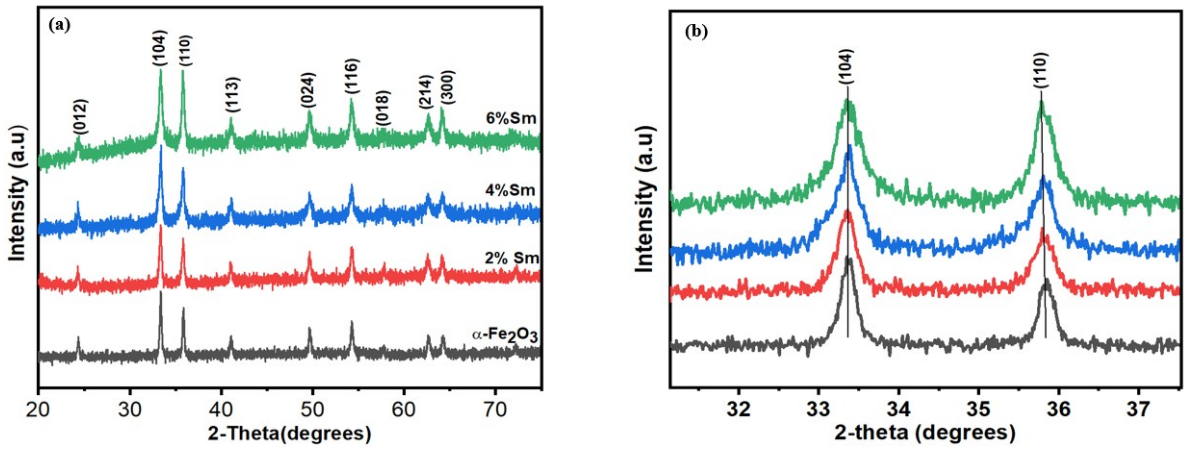

Figure 1. XRD patterns of (a) α-Fe_2O_3 and Sm-α-Fe_2O_3, and (b) Zoomed XRD for peaks (104) and (110). All samples were prepared using the hydrothermal synthesis method.

Table 1. Crystallographic parameters for undoped and Sm-doped samples.

Samples	2-theta	FWHM	D (nm)	Strain	Dislocation density
Pure	33.36	0.205	43	0.170	0.510
2 Sm	33.34	0.365	33	0.302	0.899
4 Sm	33.36	0.247	35	0.202	0.798
6 Sm	33.36	0.315	28	0.263	0.129

Based on Figure 1 (b), it is clear that doping with Sm^{3+} influences the peaks position, the broadening, and the intensity. Pure α-Fe_2O_3 has narrower peaks compared to the Sm^{3+} doped α-Fe_2O_3 NPs.Doping with various Sm^{3+} does influence the nanosize of the materials. The calculated D (nm) values decrease with the increasing Sm^{3+} percentages. Based on the previous study, the material with the smallest crystallite size has the ability to produce good results in different applications. Hence in work the smallest crystallite size was found with 6% Sm^{3+} was used as dopant, this simple mean that 6% Sm^{3+} may shows good result in appltion of this materials.

4.2. TEM analysis

Morphology of α-Fe_2O_3 and Sm^{3+}-α-Fe_2O_3 was determined using (TEM). Figure 2 represents the TEM images with the particle size of 77, 90, 119 and 115 nm for α-Fe_2O_3, 2, 4 and 6 % Sm^{3+} doped samples, respectively. The increase in the particles size for all doped samples suggest that Sm^{3+} ion incorporation promote the particle growth. Doping with various percentages of Sm^{3+} does influence the morphology as well as the particle size of the material. The α-Fe_2O_3 and 2% Sm^{3+} doped show spherical nanoparticles. However,from 4% Sm^{3+} doped, the morphology start to change from spherical nanoparticles to the nanorods, which increases in the number and size with 6% Sm^{3+} doped.

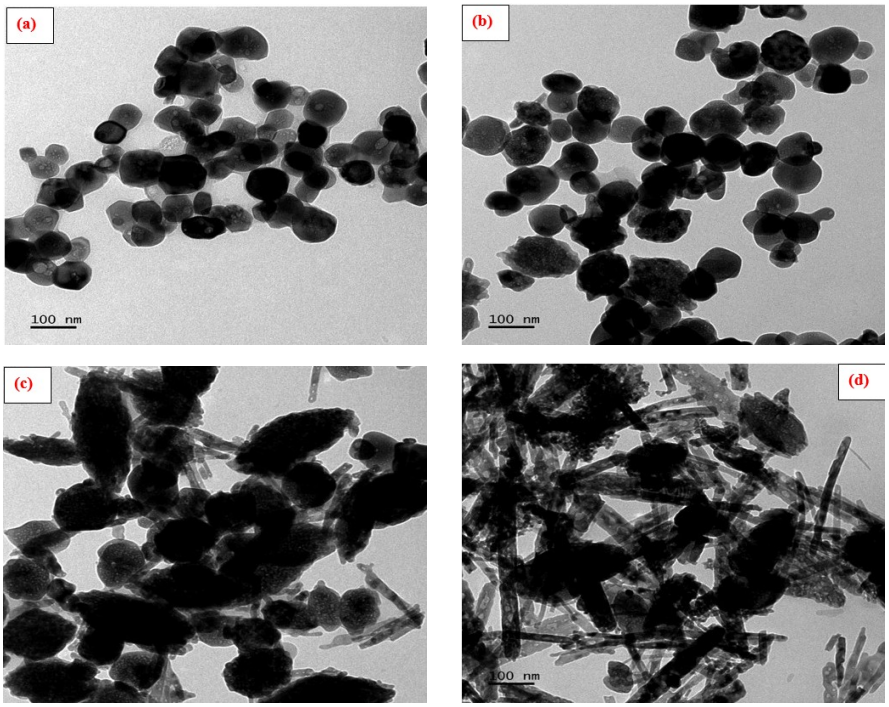

Figure 2. The (TEM) images of the (a) undoped (b) 2% Sm^{3+} (c) 4% Sm^{3+} and 6% Sm^{3+} doped α-Fe_2O_3.

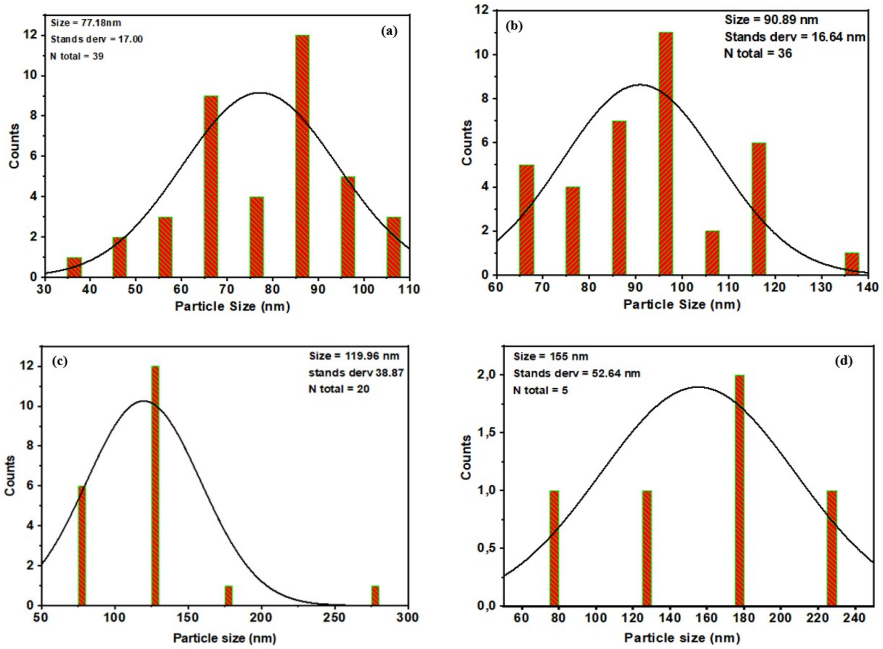

Figure 3. Particle size with fit histograms for the (a) undoped (b) 2% Sm^{3+} (c) 4% Sm^{3+} and 6% Sm^{3+} doped α-Fe_2O_3 NPs with the black line showing a lognormal fit to the data to determine average particle size.

4.3. FT-IR spectrum analysis

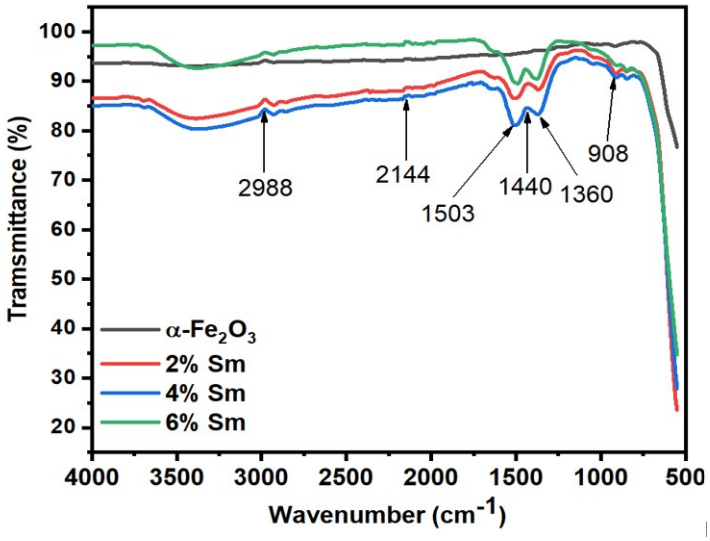

Figure 4. Plot showing the response is increasing with the operating temperature of the sensors.

The functional groups of α-Fe_2O_3 and Sm^{3+}-α-Fe_2O_3 were determined using FT-IR spectroscopy in the wavenumber range of 500–4000 cm^{-1} as shown in Figure 4. All doped samples with Sm^{3+} show almost similar trends at different transmittances. Base FT-IR spectroscopy results of materials show bonding at the following wavenumbers: 2988 cm^{-1}, 2144 cm^{-1}, 1503 cm^{-1}, and 908 cm^{-1}. The wavenumber of 2988 cm^{-1} represents the bonding between the c-H atoms, 2144 cm^{-1}, represents the triple bond between the carbon atom, 1503 cm^{-1}, represents the single bond between carbon, and the smallest wavenumber in this work confirms the formation of the vibration bond, which is between the atom Fe-O. The shifting in the transmittance is due to the effect of doping with Sm^{3+} ions.

4.4. UV-vis analysis

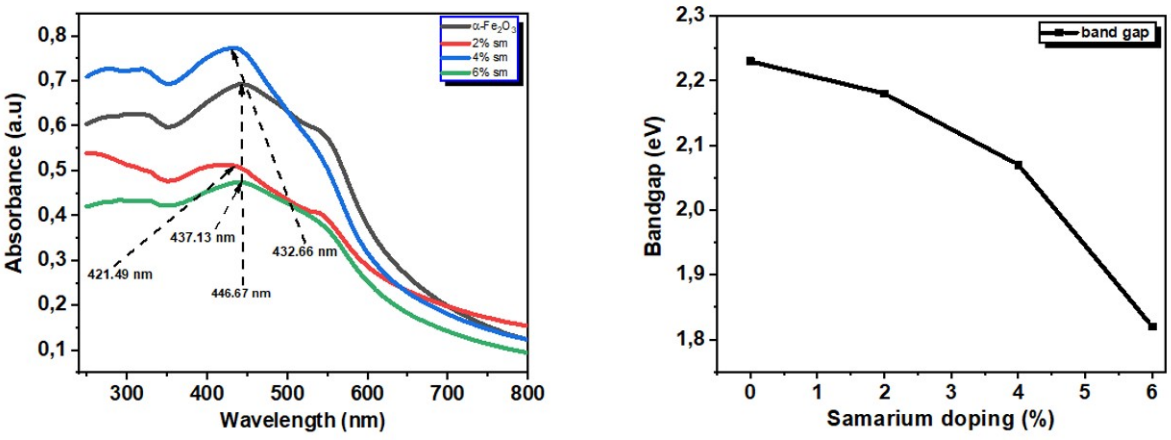

Figure 5. UV-Vis analysis of the α-Fe_2O_3 and Sm-α-Fe_2O_3 and the calculated bang gap energy.

The optical properties of undoped and doped materials with various percentages of Sm^{3+} ions were analyzed using the UV-Vis spectroscopy with the wavelength range from 200 to 800 nm. Figure 5 presents the UV-vis absorbance spectrum for the α-Fe_2O_3 NPs and Sm^{3+} doped-α-Fe_2O_3 NPs materials. The band gap energy (eV) of the individual materials was calculated using the Tauc plot method. The α-Fe_2O_3 sample shows the high band gap energy of 2.23 eV, which is in line with previous reported work on α-Fe_2O_3 NPs. However, doping with various Sm^{3+} ion leads to decrease in the bang gap values. Increasing the percentage of Sm^{3+} doping reduces the band gaps of the material from the undoped value of 2.23 to 1.81 eV at 6% Sm^{3+}. The decrease in the band gap of the material implies improved device performance, especially in gas sensing application, solar cell and in water treatment. This is mainly due to the fact that the materials has better light absorption, which also plays a role in increasing its carrier activity.

5. Conclusion

The hydrothermal method was successfully used to synthesis the α-Fe_2O_3 NPs and Sm- α-Fe_2O_3 NPs with 0-6% Sm^{3+} ions. XRD was used to further confirm the formation of α-Fe_2O_3 structure. While TEM was used to study the surface morphology of the undoped and doped materials. This study demonstrates that Sm^{3+} doping significantly influence the structural, morphological and the optical properties of hematite nanostructures. The reduction in the crystallite size, morphological transition to nanorods, and narrowed band gap highlight the enhanced potential of Sm^{3+}-doped α-Fe_2O_3 for the use in advanced application such as in gas sensors,photocatalysis, and solar energy conversation systems.

Acknowledgments

The authors acknowledge financial support from the Department of Physics and the National Research Foundation (NRF). I also like to thanks the Department of Chemistry and UKZN team characterization techniques (XRD, TEM,UV-Vis, FT-IR).

References

[1] Mirzaei, A., Hashemi, B., and Janghorban, K. *α-Fe_2O_3 based nanomaterials as gas sensors. Journal of Materials Science: Materials in Electronics*, **27**, 3109–3144 (2016).

[2] Mathevula, L. E. *Optical and Magnetic Properties of Rare Earth Doped α-Fe_2O_3 for Future Bio-Imaging Applications*, MSc Dissertation, (2018).

[3] Yousef. *Construction of Fe_2O_3/Transition Metal Dichalcogenides Heterostructures for Dyes Photodegradation.* (2023).

[4] Goel, N., Kunal, K., Kushwaha, A., and Kumar, M. *Metal oxide nanostructures-based gas sensors. Authorea Preprints*, (2022).

[5] Zhou, R., Lin, X., Xue, D., Zong, F., Zhang, J., Duan, X., Li, Q., and Wang, T. *Enhanced H_2 gas sensing properties by Pd-loaded urchin-like $W_{18}O_{49}$ hierarchical nanostructures. Sensors and Actuators B: Chemical*, 900–907 (2018).

[6] Zhang, X., Li, H., Wang, S., Fan, F.-R. F., and Bard, A. J. *Improvement of hematite as photocatalyst by doping with tantalum. The Journal of Physical Chemistry C*, 16842–16850 (2014).

[7] Ramadhan, S. F., Muheb, A. S., and Ramadhan, R. A. *Characterization study of synthetic iron oxide nanoparticles at different temperature. International Journal of Current Engineering and Technology*, 1686 (2013).

[8] Nasiri, S., Rabiei, M., Palevicius, A., Janusas, G., Vilkauskas, A., Nutalapati, V., and Monshi, A. *Modified Scherrer equation to calculate crystal size by XRD with high accuracy, examples Fe_2O_3, TiO_2 and V_2O_5. Materials Chemistry and Physics*, 100015 (2023).